Supplementary Information

Electrosynthesis of hydrogen peroxide with anion exchange membrane-free resin wafer reactors

Chaoyong Sun[1,2], Jiaqiang Zhong[1,2], Erzhuo Zhao[1,2], Yujue Wang[1,2,3 *]

[1] School of Environment, Tsinghua University, 100084 Beijing, China

[2] State Key Laboratory of Regional Environment and Sustainability, Tsinghua University, 100084 Beijing, China

[3] Beijing Key Laboratory for Emerging Organic Contaminants Control, Tsinghua University, 100084 Beijing, China

[*] Corresponding author: Yujue Wang, E-mail: wangyujue@tsinghua.edu.cn

S1. Resin wafer, wafer reactor, and experimental systemd for H_2O_2 electrosynthesis

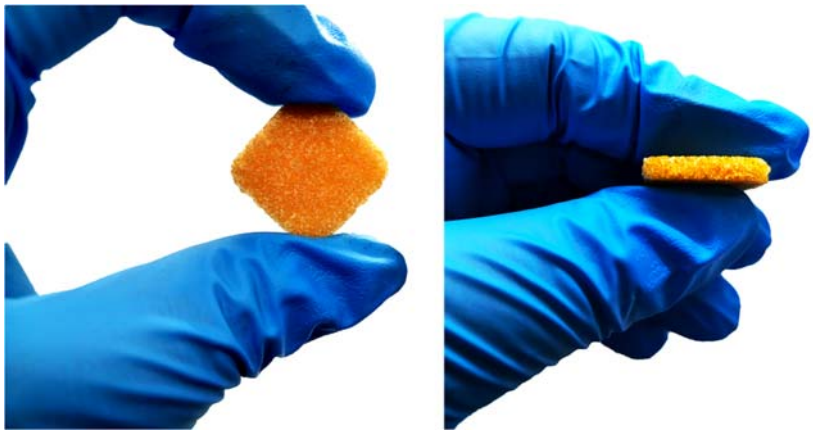

Fig. S1. Front and side views of a resin wafer (2 cm × 2 cm × 0.2 cm)

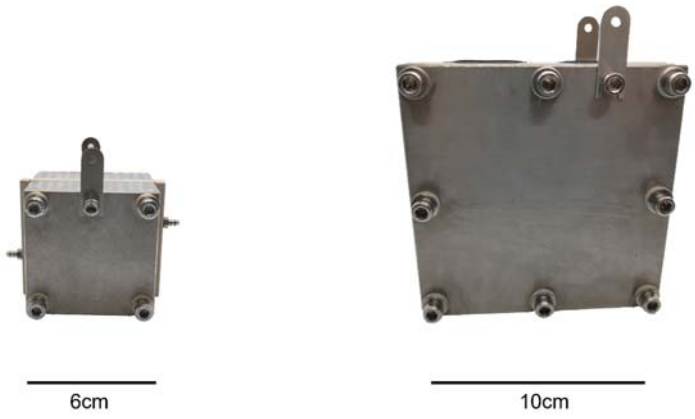

Fig. S2. Photos of the 4 cm² and 25 cm² resin wafer reactors

Fig. S3. The experimental system for H_2O_2 electrosynthesis

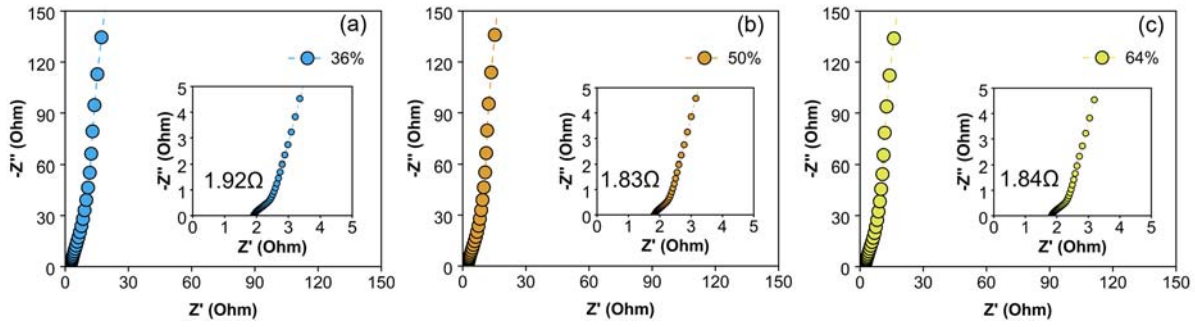

Fig. S4. Nyquist plots of resin wafers fabricated with varying mixing ratios of resin microspheres, pore forming agent, and binder (a) 5 (g):9 (g):1 mL, (b) 7 (g):7 (g):1 mL, and (c) 9 (g):5 (g):1 mL.

S2. Effects of packing density of resin microspheres on H_2O_2 electrosynthesis

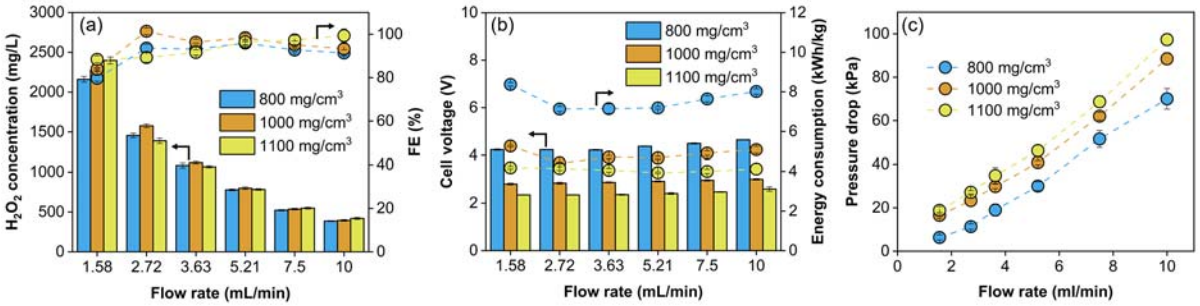

Fig. S5. Effects of packing density of resin microsphere on (a) H_2O_2 concentrations and FEs of H_2O_2 production, (b) cell voltages and electric energy consumption of H_2O_2 production, and (c) pressure drop during H_2O_2 electrosynthesis with the microsphere-backed reactor (4 cm^2 electrode) in the continuous flow mode.

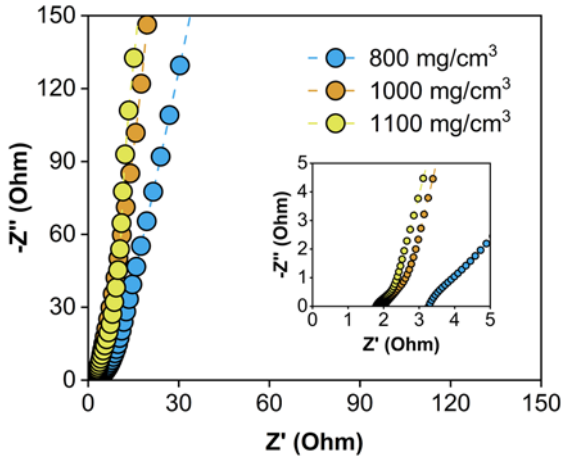

Fig. S6. Nyquist plots of resin microsphere-packed beds of varying packing densities.

S3. Stability of AEM during H_2O_2 electrosynthesis

Fig. S7 shows the photos of AEM used in the microsphere-packed reactor before and after the stability experiments (see Fig. 2d for more detail). The original AEM was a thin, smooth film. However, numerous pits are observed on the surface of used AEM. Because of the high water pressures inside the microsphere-packed reactor, the three chambers of the reactor had to be firmly bolted together to prevent water leakage during operation. As a result, the resin microsphere-packed bed was tightly pressed against the AEM under high pressures [1,2]. This can cause significant mechanical damage to the AEM, as evidenced by the numerous pressure-induced pits on the surface of used AEM (see Fig. S7d). Moreover, HO_2^- can attack the quaternary ammonium group of AEMs, thus causing chemical degradation of AEMs [2]. Consequently, AEMs will be gradually decomposed during H_2O_2 electrosynthesis, posing a critical barrier to the long-term stability of microsphere-packed reactor [1-3].

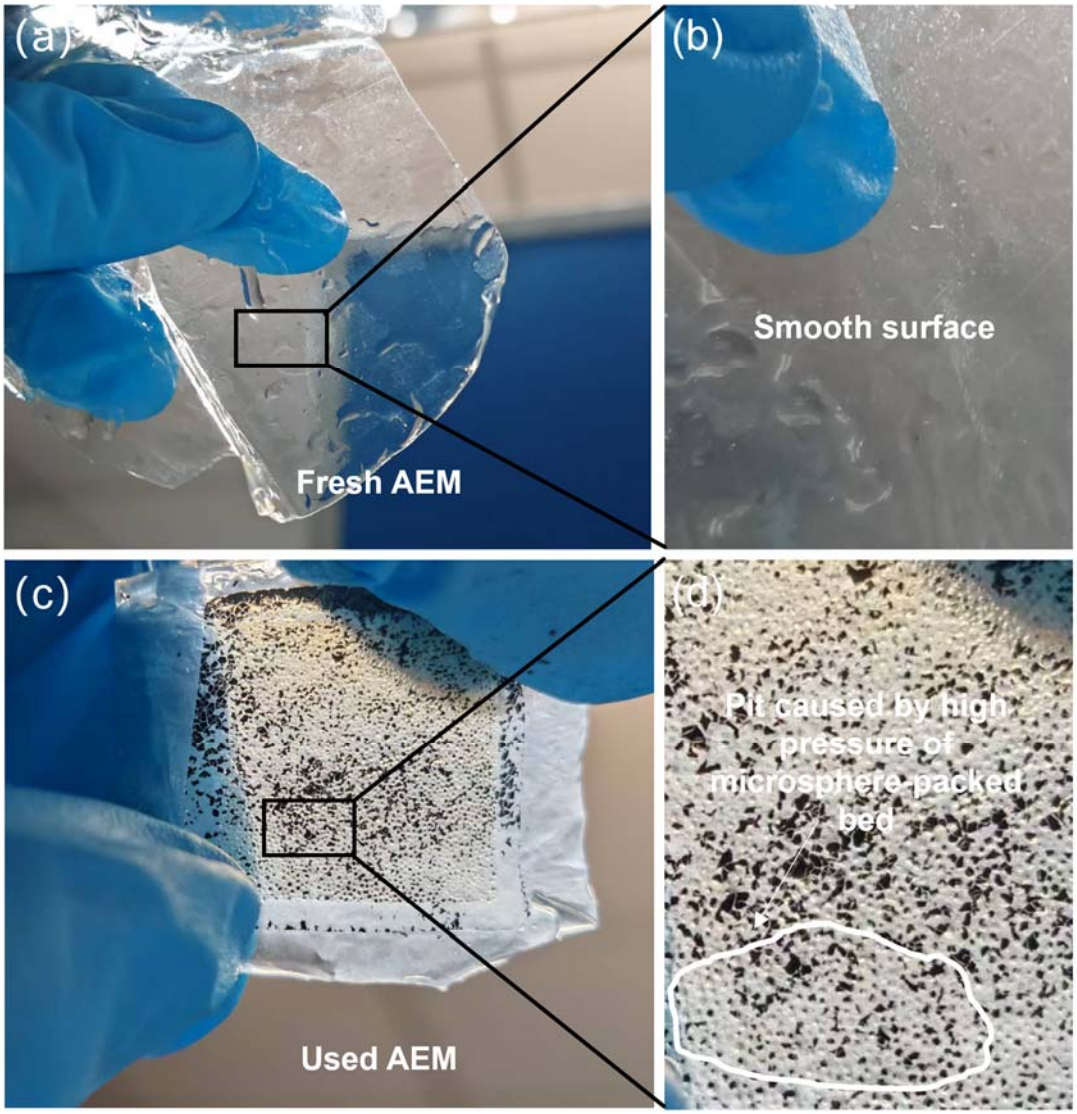

Fig. S7. Photos of AEMs (a, b) before and (c, d) after used for H_2O_2 electrosynthesis in the resin microsphere-packed reactor.

S4. Effects of current density on H_2O_2 electrosynthesis

Fig. S8 shows the effects of applied current density on H_2O_2 electrosynthesis with the resin microsphere-packed reactor and resin wafer reactor in the continuous flow mode. During the experiments, the applied current densities were stepwise increased every 15 min. Corresponding to the increases of current densities, the concentrations of produced H_2O_2 solutions increased monotonically (Fig. S8a). FEs of H_2O_2 production remained generally >80% for the microsphere-packed reactor and >90% for the wafer reactor within the test current density range. On the other hand, cell voltages increased with increasing current densities (Fig. S8b). As a result, the electric energy consumption of H_2O_2 production increased with increasing current densities. Notably, the pressure drops across the microsphere-packed reactor increased substantially during the experiments, although the water flow rate was kept constantly at 1.58 mL/min. These increases can be mainly attributed to the generation and accumulation of oxygen gas bubbles in the microsphere-packed reactor due to the small porosity of resin microsphere-packed bed (see the discussion of Fig. 4c in the main text). In contrast, gas bubbles can be quickly removed from the wafer reactor because of the higher porosity of resin wafer. Therefore, the pressure drops across the wafer reactor changed insignificantly during the experiments.

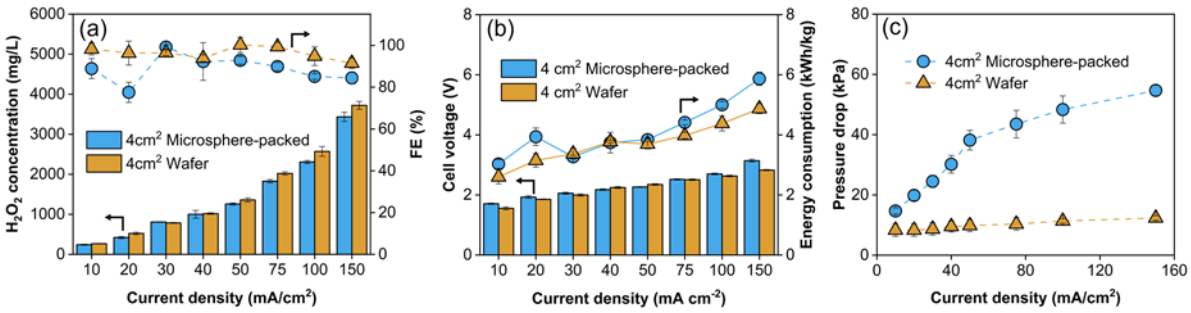

Fig. S8. Effects of current density on (a) H_2O_2 concentrations and FEs of H_2O_2 production, (b) cell voltages and electric energy consumption of H_2O_2 production, and (c) pressure drop during H_2O_2 electrosynthesis with the microsphere-backed reactor and PSE wafer reactor (4 cm^2

electrode) in the continuous flow mode.

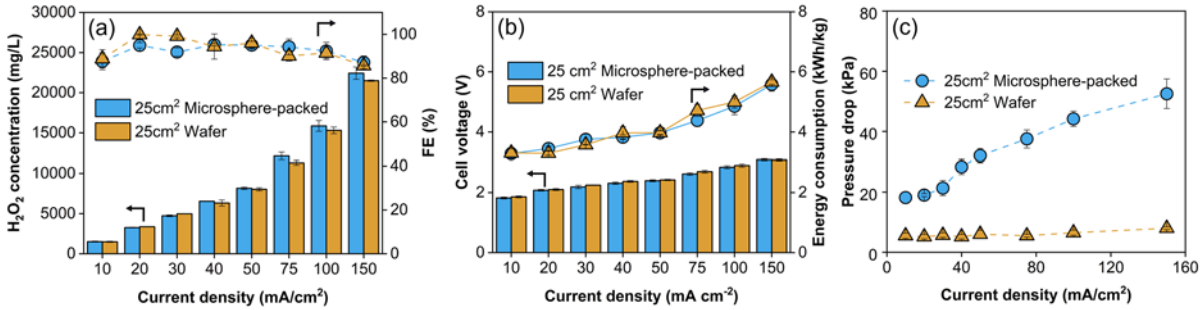

Fig. S9. Effects of current density on (a) H_2O_2 concentrations and FEs of H_2O_2 production, (b) cell voltages and electric energy consumption of H_2O_2 production, and (c) pressure drop during H_2O_2 electrosynthesis with the microsphere-backed reactor and PSE wafer reactor (25 cm^2 electrode) in the continuous flow mode.

S5. FEs and electric energy consumption during H_2O_2 electrosynthesis in the recirculating mode

The FEs and electric energy consumption during H_2O_2 electrosynthesis with the resin wafer reactor in the recirculating operation are calculated and compared to the results reported for conventional electrochemical reactor using aqueous electrolytes and resin microsphere-packed reactors in recent literature (see Table S1).

Table S1. Comparison of electrochemical reactors for H_2O_2 electrosynthesis.

Electrolyte	j (mA/cm^2)	Cell voltage (V)	H_2O_2 conc. (wt. %)	FE (%)	EC (kWh/kg H_2O_2)	Ref
0.1 M Na_2SO_4	100	2.75	1.00	78.8	5.50	[4]
0.5 M Na_2SO_4	200	2.75	0.93	62.5	6.93	[5]
1M Na_2SO_4	300	2.57	4.60	84	4.82	[6]
1 M Na_2SO_4	50	2.21	1.20	75.6	4.61	[7]
	100	2.53	2.13	67.1	5.95	
	150	3.14	2.87	60.2	8.23	
	200	3.68	3.41	53.8	10.79	
1M NaCl	100	4.78	1.00	70	10.76	[8]
1M NaCl	1000	6.40	-	75.6	13.34	[9]
1M KOH	100	4.20	1.52	96	6.90	[10]
	150	4.90	2.05	75	10.30	
	200	-	2.66	60	-	
1M KOH	200	-	2.80	65	-	[11]
Resin microsphere-packed bed (2 cm × 2 cm)	68	4.00	2.70	96	6.57	[12]
Resin microsphere-packed bed (5 cm × 5 cm)	100	2.77	0.40	80	5.46	[13]
Resin microsphere-packed bed (2 cm × 2 cm)	100	2.30	2	70	5.17	[14]
Resin microsphere-packed bed (2 cm × 2 cm)	100	5.00	2.0	80	9.46	[15]
	100	4.80	4.0	75	11.14	
	100	5.00	10.0	70	11.26	
	100	5.50	12.0	65	13.33	
Resin microsphere-packed bed (5 cm × 5 cm)	100	4.56	9.25	77.7	9.23	This work
Resin wafer (5 cm × 5 cm)	100	3.57	10.97	92.3	6.10	This work

S6. Pumping energy consumption during H_2O_2 electrosynthesis

Pumping energy consumption of H_2O_2 production (kWh/kg H_2O_2) is calculated based on the pressure drops across the reactor and concentrations of H_2O_2 product using Eq. S1.

$$E_{pump} = \frac{\triangle P}{3.6c} \qquad \text{(S1)}$$

where E_{pump} is the pumping energy consumption of H_2O_2 production (kWh/kg H_2O_2), $\triangle$P is the pressure drop across the reactor (kPa), and c is the H_2O_2 concentration (mg/L).

During H_2O_2 electrosynthesis in the continuous flow mode, the concentrations of H_2O_2 effluent decrease, while the pressure drops across the reactor increase with increasing flow rates (see Fig. 2c and Fig. 3c). Therefore, the pumping energy consumption increased significantly with flow rates (Fig. S10 and Fig. S11). This finding suggests that it would be more economical to operate the PSE reactor at relatively low flow rates during H_2O_2 electrosynthesis. However, low flow rates are not beneficial to quickly transport the produced H_2O_2 away from the cathode surface, which may aggravate H_2O_2 reduction to H_2O. This parasite reaction will decrease FEs, and thus increases the electric energy consumption of H_2O_2 production. Therefore, in practical operations, the flow rates should be systematically optimized to minimize the overall energy consumption. In fact, the results shown herein indicate that compared with the electric energy consumption (~4 kWh/kg H_2O_2, see Fig. 2b), the pumping energy consumption is almost negligible (0.01–0.1 kWh/kg H_2O_2). Therefore, more attention should possibly be paid to maintaining high FEs and thus minimizing the electric energy consumption of H_2O_2 production when optimizing the flow rates during H_2O_2 electrosynthesis.

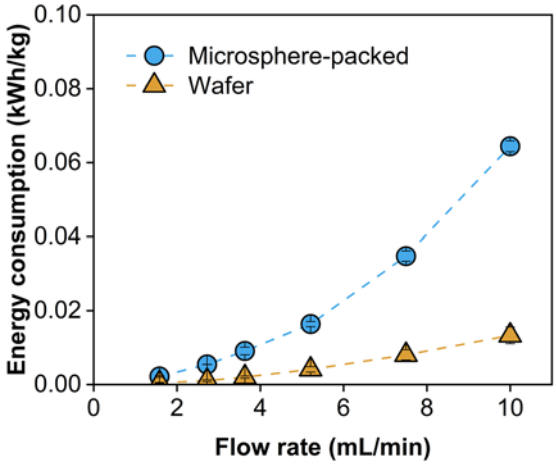

Fig. S10. Pumping energy consumption as a function of water flow rates during H_2O_2 electrosynthesis with the microsphere-backed reactor and PSE wafer reactor (4 cm^2 electrode) in the continuous flow mode.

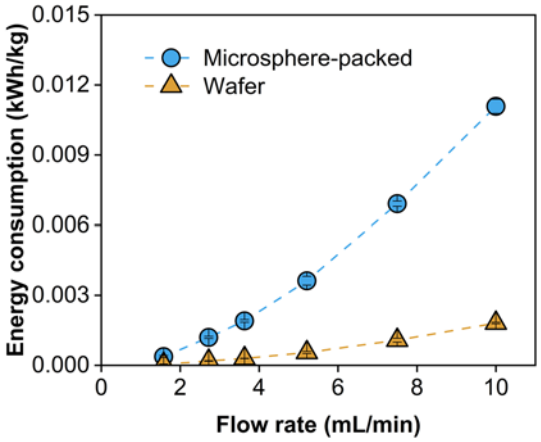

Fig. S11. Pumping energy consumption as a function of water flow rates during H_2O_2 electrosynthesis with the microsphere-backed reactor and PSE wafer reactor (25 cm^2 electrode) in the continuous flow mode.

References

1 Xia, Y., Zhu, P., Yang, Y. L., Qiu, C. & Wang, H. T. Electrochemical Manufacturing of Hydrogen Peroxide with High Concentration and Durability. *Acs Catal* **15**, 4560-4569, doi:10.1021/acscatal.4c07033 (2025).

2 Zhao, E. *et al.* Optimization and scaling-up of porous solid electrolyte electrochemical reactors for hydrogen peroxide electrosynthesis. *Nature Communications* **16**, 3212, doi:10.1038/s41467-025-58385-2 (2025).

3 Shin, H., Lee, S. & Sung, Y. E. Industrial-scale H2O2 electrosynthesis in practical electrochemical cell systems. *Curr Opin Electroche* **38**, doi:10.1016/j.coelec.2023.101224 (2023).

4 Jia, S. *et al.* Modulated Nickel Single-Atom Sites as Highly Active Catalysts for the Synthesis of Neutral H2O2 at Ampere-Level Current Densities. *ACS Nano* **19**, 22402-22413, doi:10.1021/acsnano.5c06049 (2025).

5 Liu, C. *et al.* Heterogeneous molecular Co–N–C catalysts for efficient electrochemical H2O2 synthesis. *Energy & Environmental Science* **16**, 446-459, doi:10.1039/d2ee02734h (2023).

6 Lee, B.-H. *et al.* Supramolecular tuning of supported metal phthalocyanine catalysts for hydrogen peroxide electrosynthesis. *Nature Catalysis* **6**, 234-243, doi:10.1038/s41929-023-00924-5 (2023).

7 Zhao, E. *et al.* Technoeconomic Assessment of Electrochemical Hydrogen Peroxide Production with Gas Diffusion Electrodes under Scenarios Relevant to Practical Water Treatment. *ACS ES&T Engineering* **3**, 1800-1812, doi:10.1021/acsestengg.3c00238 (2023).

8 Sang, Z. *et al.* Internal hydrogen-bond enhanced two-electron oxygen reduction reaction for π-d conjugated metal-organic framework to H2O2 synthesis. *Nature Communications* **16**, doi:10.1038/s41467-025-58628-2 (2025).

9 Nie, J. *et al.* Accelerating water dissociation to achieve ampere-level hydrogen peroxide electrosynthesis in brine and seawater. *Nature Communications* **16**, doi:10.1038/s41467-025-60950-8 (2025).

10 Cao, P. *et al.* Metal single-site catalyst design for electrocatalytic production of hydrogen

peroxide at industrial-relevant currents. *Nature Communications* **14**, doi:10.1038/s41467-023-35839-z (2023).

11 Bao, Z. *et al.* Ni3V2O8 Nanospheres for Sustained and Efficient Enhancement of Electrocatalytic H2O2 Production in pH-Universal Solutions. *ACS Catalysis* **14**, 12140-12151, doi:10.1021/acscatal.4c02945 (2024).

12 She, F. *et al.* Curvature-Dependent Electrochemical Hydrogen Peroxide Synthesis Performance of Oxidized Carbon Nanotubes. *ACS Catalysis* **14**, 10928-10938, doi:10.1021/acscatal.4c01637 (2024).

13 Zhao, E. *et al.* Optimization and scaling-up of porous solid electrolyte electrochemical reactors for hydrogen peroxide electrosynthesis. *Nature Communications* **16**, doi:10.1038/s41467-025-58385-2 (2025).

14 Wang, J. *et al.* Catalyst-Engineered Proton Transfer Pathways for Selective Hydrogen Peroxide Electrosynthesis in Solid-State Electrolytes. *Angewandte Chemie International Edition* **64**, doi:10.1002/anie.202510645 (2025).

15 Xia, Y., Zhu, P., Yang, Y., Qiu, C. & Wang, H. Electrochemical Manufacturing of Hydrogen Peroxide with High Concentration and Durability. *ACS Catalysis* **15**, 4560-4569, doi:10.1021/acscatal.4c07033 (2025).